Input Impedance of a Coaxial Line Terminated With a Complex Gap Capacitance—Numerical and Experimental Analysis

J. Obrzut and A. Anopchenko

***Abstract*—A full-wave numerical analysis was performed for a coaxial line terminated with a complex gap capacitance using a finite-element high-frequency structure simulator. The scattering parameters, input impedance, and spatial distribution of the electromagnetic field have been obtained in the frequency range of 100 MHz to 19 GHz for specimens 8 to 320 μm thick, with a dielectric constant of up to 80. It was found that the residual inductance of the specimen affects the impedance characteristic of the network. The inductance-capacitance resonance is coupled with the cavity resonance. The specimen inductance is linearly dependent on the specimen thickness. At frequencies near the cavity resonance, the specimen section can be treated as a network of a transmission line with a capacitance, where the fundamental mode propagates along the diameter of the specimen. Results of the numerical analysis were verified experimentally using water as a model material with a high dielectric constant. Our closed-form formula for input impedance of the network is valid in a wider frequency range than the lumped-element method. The results are useful in improving the accuracy of broadband dielectric measurements in the extended frequency range of thin films with high dielectric constant that are of interest to bio- and nanotechnology.**

***Index Terms*—Coaxial discontinuity, dielectric materials, full-wave analysis, high-frequency electromagnetic simulation, high-frequency measurements.**

I. Introduction

THE relationship between the structure, function, and stability of proteins and other biological substances has become an important research area of bio- and nanotechnology. It is widely recognized that protein function depends on molecular structural arrangement which dynamically changes with relaxation times in the subnanosecond range [1]. Broadband dielectric measurements are well suited for studying structural relaxation dynamics of such materials that typically exhibit a high dielectric constant, and are available in small quantities. In these applications the frequency range of interest extends into the microwaves, above 5 GHz.

Iskander and Stuchly proposed a highly refined technique for measuring the broadband dielectric properties of biological materials from the reflection coefficient. As a sample holder, they used a small-gap shunt capacitor terminating a coaxial line [2]. This technique is accurate at frequencies where the sample holder can be treated as a lumped capacitance. They empirically determined that this technique is accurate up to a frequency at which input impedance of the specimen decreases to one-tenth (0.1) of the characteristic impedance of the coaxial line [3]. This frequency limit is lower for specimens that have a higher dielectric constant. For a 100-μm-thick specimen with a dielectric constant of about 60, measured in the Amphenol Precision Connector 7 mm (APC-7) configuration, the upper frequency limit falls to within 85 MHz. This is well below the desirable frequency range of about 5–20 GHz.

Marcuvitz analyzed an equivalent circuit of a coaxial line, terminated by a small gap capacitance, treating it as a quasi-electrostatic problem. His analysis assumes a principal propagating mode in the coaxial line and no propagation in the gap [4]. However, wave propagation has been observed experimentally in thin-film specimens with a high dielectric constant [5]. Analysis of the fundamental mode in the specimen section was performed, treating the specimen as a network consisting of a transmission line with a capacitance. This led to a correction procedure that allowed extending the usable frequency range to about 8 GHz [5].

A more fundamental analysis of the transverse electromagnetic wave scattering in a coaxial line terminated by a gap was performed by Eom *et al.* using a Fourier transform and mode matching technique [6]. The complex input gap impedance was calculated by Davidovich using full-wave spectral-domain analysis [7]. The results agreed with the Marcuvitz model up to frequencies of 12 GHz, but no satisfactory physical solution was obtained for gaps thinner than 100 μm and a dielectric constant larger than ten.

In this paper we present a full-wave numerical analysis of the coaxial line terminated by a complex gap capacitance. The problem was formulated without any prior assumptions about the properties of the network equivalent circuit. The scattering parameters, input impedance, and spatial distribution of the electromagnetic field have been obtained in the frequency range of 100 MHz to 19 GHz for specimens 8 to 320 μm thick, with a dielectric constant of up to 80. Numerical simulations were verified experimentally using water as a dielectric material filling the gap.

Manuscript received June 15, 2003; revised April 22, 2004. Certain commercial materials and equipment are identified in this paper in order to adequately specify the experimental procedure and do not imply recommendation by the National Institute of Standards and Technology nor does it imply that the materials or procedures are the best for these purposes.

The authors are with the Polymers Division, National Institute of Standards and Technology, Gaithersburg, MD 20899 USA.

Digital Object Identifier 10.1109/TIM.2004.830777

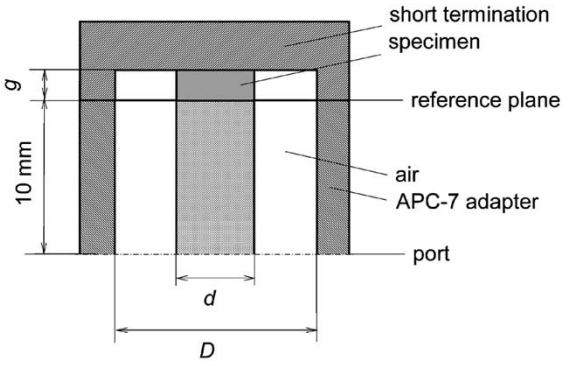

Fig. 1. Schematic representation of the test fixture.

II. Analysis and Measurements

A. Numerical Model

The three-dimensional field solution of Maxwell's equations was obtained using a finite-element high frequency structure simulator (HFSS) from Ansoft. The geometrical model of the network consisted of a 50-Ω 10-mm-long lossless coaxial line (Fig. 1). In Fig. 1, d and D denote diameter of the line inner and outer conductor, respectively. The specimen was represented by a dielectric gap of thickness g added to the central conductor and short terminated on the other side. The gap contained a dielectric having complex permittivity $\varepsilon^* = \varepsilon' - j\varepsilon''$. The conducting surfaces at the dielectric were assumed to have the conductivity of copper. The reference plane was set at the beginning of the coaxial line, and then after calculations, it was de-embedded to the position shown in Fig. 1. The geometric model was divided into about 40 000 tetrahedra elements as a finite-element mesh. By representing the electric and magnetic field as a combination of finite quantities in each tetrahedron, Maxwell's equations were transformed into matrix equations that could be solved by traditional numerical methods. HFSS utilizes a self-adaptive mesh generation procedure in which the mesh is refined in regions of high error density. The computational error is estimated using the concept of successive error function that uses trial electric and magnetic fields for each element of the mesh [8]. The mesh is refined by subdividing only those elements having the largest errors. The adaptive mesh was grown approximately 20% each iteration of the mesh refinement process. After calculating the electric and magnetic fields, the scattering parameter S_{11} of the network was obtained by comparing energy of the incoming and outgoing waves through the port located at the reference plane. The adaptive solution was stopped when the change in the scattering parameter was less than 10^{-4}. The uncertainty in the S_{11} parameter was $\pm 10^{-4}$. The corresponding uncertainty of the impedance results normalized to 50 Ω was $\pm 10^{-2}$ Ω.

B. Experimental Setup

Results of numerical analysis were verified experimentally using a coaxial test fixture depicted in Fig. 1. The test fixture was constructed from an APC-7 to an APC-3.5 microwave adapter. The center conductor was replaced with a fixed 3.0-mm-diameter pin, machined precisely to achieve a flat and parallel contact between the film specimen and the APC-7 standard short termination. The diameter of the outer conductor D was made 7.0 mm. One-port measurements of the scattering parameter S_{11} were carried out using a network analyzer HP 8720D. Open, short, and broadband load calibration was performed using an Agilent 85 050B 7 mm calibration kit. For the purpose of this experiment we obtained several separate short termination standards. In each short, a different size gap was custom ground to accommodate dielectric specimens of different thickness. During measurements of water, the gap was filled with deionized water of conductivity ≤ 2 μS/cm obtained from Fluka. An appropriate volume was dispensed with an electronic micropipette EDP2 from Rainin. For example, a 240-μm-thick film corresponded to approximately 1.8 μl. The measurements were performed in the frequency range of 100 MHz to 12 GHz. No reliable results were obtained above 12 GHz, probably due to dimensional imperfections in the experimental test fixture. The temperature of the water specimen was about 30 °C. The relative combined standard uncertainty in geometrical capacitance measurements was 4%. The largest contributing factor to the uncertainty was the uncertainty in measuring the thickness of the film. This uncertainty was 10 μm. The relative standard uncertainty of S_{11} was assumed to be within the manufacturer's specification for the network analyzer. The combined relative experimental uncertainty in complex impedance was within 10%, while the experimental resolution was about ±0.05 Ω.

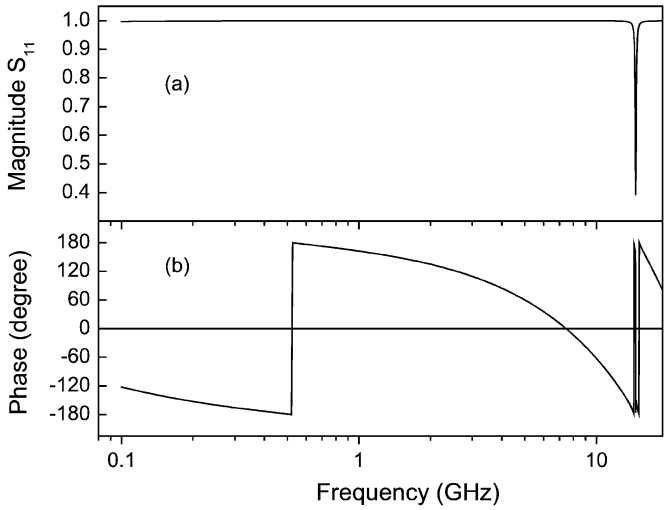

Fig. 2. Scattering parameter S_{11} at the port reference plane for a 10-mm-long APC-7 coaxial line terminated with a 80-μm-thick gap. The gap is filled with a dielectric of permittivity $69.2 - j\ 0.16$. (a) Magnitude and (b) phase.

III. Results and Discussion

A. Model Calculations and Analysis

The magnitude and phase of the S_{11}-parameter, calculated in the frequency range of 100 MHz to 19 GHz for the 10-mm-long coaxial line with a thin dielectric film specimen as a load, is shown in Fig. 2. The complex permittivity of the specimen is $69.2 - j\ 0.16$ and its thickness is 80 μm. The magnitude plot of S_{11} shows a minimum at frequency f_{cav} of 14.6 GHz. This feature originates from the primary cavity resonance in the specimen section. The 360° change in the phase shift

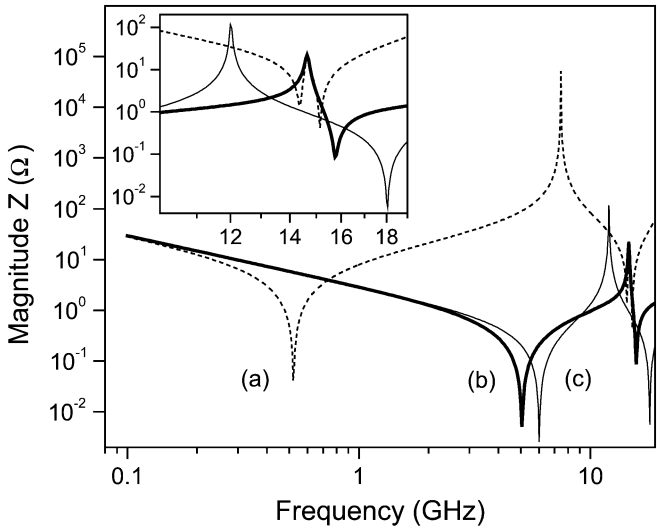

Fig. 3. Impedance versus frequency. (a) Before deembedding the coaxial line section, (b) after deembedding, and (c) calculated from (1). Details of the impedance characteristic near the cavity resonance are shown in the inset.

at about 520 MHz indicates that the network exhibits an inductance-capacitance *(LC)* series resonance at this frequency. Above 520 MHz the network's character changes from capacitive to inductive. This frequency agrees well with the resonant frequency calculated from the circuit parameters—the inductance of the 10-mm-long coaxial line ($L_{\rm line} = 1.69$ nH) and the lumped capacitance C_M of the Marcuvitz equivalent circuit [4] ($C_M = 54.1$ pF). Fig. 3(a) shows the corresponding plot of impedance at the reference plane, where $|Z|$ has a sharp minimum, resulting from the *LC* resonance at 520 MHz. As the frequency increases, the phase shift of S_{11} approaches zero at about 7.8 GHz [Fig. 2(b)] and the corresponding magnitude of impedance reaches a subsequent maximum [Fig. 3(a)] at that frequency.

The effect of the transmission line can be deembedded by transforming the scattering parameter S_{11} from the port terminal to a new reference plane, located at the interface between the end of the center conductor and the specimen. The input impedance of the specimen, determined from the transformed S_{11}, is shown in Fig. 3(b). It is seen that the frequency of the *LC* resonance has shifted from 520 MHz to 5.05 GHz. Now, in effect, the *LC* resonance is coupled to the primary cavity resonance. The cavity resonant frequency of 14.6 GHz remains unchanged by this transformation.

The input impedance of the specimen, calculated according to the model developed earlier [5], [9], (1), is plotted in Fig. 3(c) assuming $L = 0$

$$Z_{\rm in} = \frac{x\cot(x)}{j\omega C_M} + j\omega L. \tag{1}$$

Here C_M is the lumped capacitance, L is the residual inductance due to finite thickness of the specimen section, $\omega = 2\pi f$ is the angular frequency, and $x = \omega l\sqrt{\varepsilon^*}/2c$. The specimen section in (1) represents a transmission line with a capacitance having a propagation length l, $l = (c/f_{\rm cav}\,{\rm Re}(\sqrt{\varepsilon^*}))$. At low frequencies when $x \ll 1$, the inductance term L can be neglected, the value of the $x\cot(x)$ approaches unity, and then (1) simplifies to the input impedance of a coaxial line terminated with a shunt capacitance. For the specimen with complex permittivity of $69.2 - j\,0.16$, the propagation term of (1), $x\cot(x)$, is zero at frequency of 6.0 GHz when $x = \pi/2$, followed by a singularity at 12 GHz, when $x = \pi$. Consequently, $|Z_{\rm in}|$ has a corresponding minimum and maximum at these frequencies [Fig. 3(c)]. The difference between the frequency $f_{\rm LC}$ of the first resonance in Fig. 3(b) at 5.05 GHz and that corresponding to the first minimum in Fig. 3(c) at 6.0 GHz can be rationalized as resulting from the residual inductance L. This inductance is included in the full-wave numerical results plotted in Fig. 3(b), but neglected in the model represented by (1) with $L = 0$. The series inductance L can be rationalized based on our results of numerical analysis (Fig. 2) and the equivalent circuit of a TM mode proposed by Belhadj-Tahar *et al.* [10] to model the series resonance area.

TABLE I
FREQUENCY OF THE *LC* ($f_{\rm LC}$) AND CAVITY ($f_{\rm cav}$) RESONANCE IN RELATION TO THE DIAMETER d THICKNESS g, AND PERMITTIVITY ε^*, OF THE SPECIMEN

d (mm)	g (μm)	ε^*	C_M (pF)	L (pH)	f_{LC} (GHz)	f_{cav} (GHz)
3 (APC-7)	8	34.6 - *j*1.6	271	0.92	7.35	20.2
3 (APC-7)	80	34.6 - *j*1.6	27.1	9.71	7.25	20.6
3 (APC-7)	320	34.6 - *j*1.6	6.77	39.9	7.2	20.6
6 (APC-14)	320	34.6 - *j*1.6	27.1	39.9	3.6	10.3
3 (APC-7)	80	69.2 - *j*1.6	54.2	10.3	5.05	14.6
3 (APC-7)	80	69.2 – *j*0.16	54.2	10.3	5.05	14.6

It has been commonly accepted that for thin-film specimens the inductive component is negligibly small, and the electrical characteristic of the gap specimen is dominated by its complex capacitance. Most of analytical work on coaxial discontinuities applied this assumption to simplify the corresponding theoretical model [11]–[13]. However, the results presented in Fig. 3(b) indicate that the residual inductance of the specimen can considerably influence the impedance characteristic, especially at higher frequencies. In order to analyze this effect in more detail, we calculated the input impedance in relation to the film thickness, its diameter, and the dielectric permittivity. The results are summarized in Table I. The L values were calculated from (1) using resonance frequency values obtained with HFSS. Table I shows that for a given geometric configuration and permittivity the $f_{\rm LC}$ remains independent of the film thickness. For example, in the APC-7 configuration, and at a permittivity of $34.6 - j1.6$, the $f_{\rm LC}$ is about 7.3 GHz, while the specimen thickness increases from 8 to 320 μm. Therefore, the inductance L can be determined from the value of the $f_{\rm LC}$. In this example, when the specimen's thickness decreases from 80 to 8 μm, L decreases by a factor of ten. However, the capacitance C_M increases by the same factor. Thus, the resonant frequency $f_{\rm LC}$, which corresponds to the minimum value of the input impedance, remains unchanged. This finding indicates that the residual inductance is linearly dependent on the specimen's thickness. An analogous conclusion was arrived at by Belhadj-Tahar *et al.* [10], who developed and analyzed an equivalent circuit model of the circular waveguide filled with a dielectric material. In this new model, the equivalent circuit of a TM mode was taken as a starting point. The solution obtained for the equivalent circuit indicates that the inductance can be expressed as a reciprocal function of Marcuvitz's parallel-plate capacitance [10]. This result supports our finding with respect to the thickness dependence of the

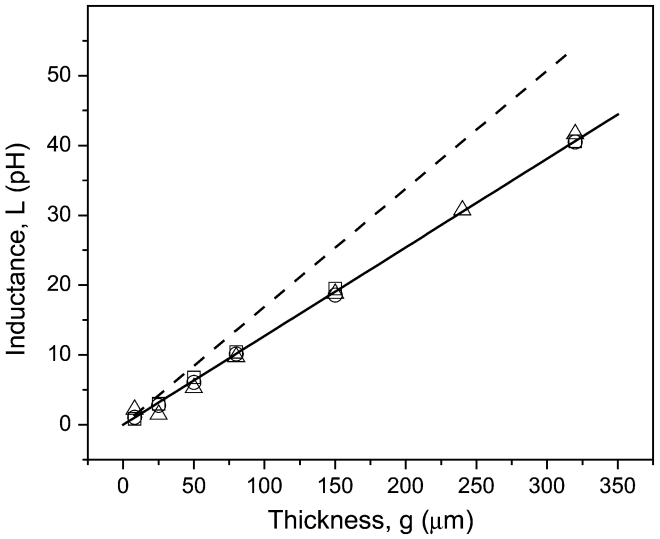

Fig. 4. Model inductance as a function of thickness of the gap. The gap is filled with a dielectric of permittivity 10 (squares), 40 (circles), and 80 (triangles). The dashed line represents inductance of a lossless air-filled coaxial line.

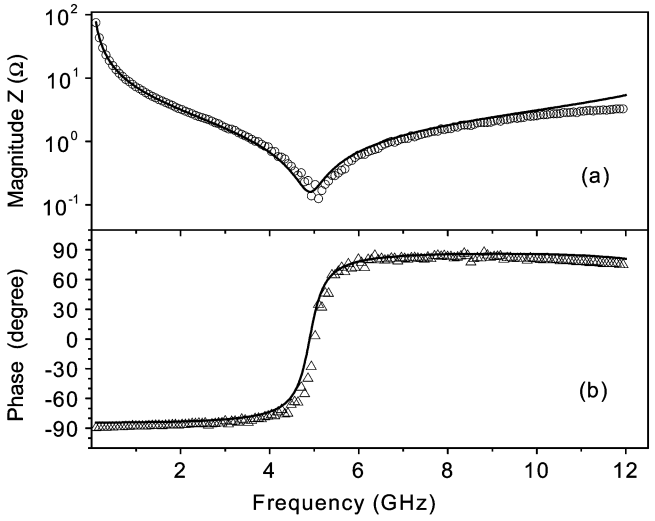

Fig. 5. Impedance characteristic measured at 30 °C (circles) and calculated (line) for a 240 μm thick water specimen with permittivity of $76-j6$. (a) Magnitude and (b) phase.

residual inductance. Fig. 4 illustrates that L increases linearly with specimen thickness according to the following equation:

$$L = B_L\, g \tag{2}$$

where $B_L = (1.27 \pm 0.01)10^{-7}$ H/m is the model inductance per unit length and g is the specimen thickness. Due to a high aspect ratio between the specimen diameter and its thickness, the results of HFSS numerical simulations are somewhat less accurate for $g < 20$ μm, which leads to larger uncertainty in B_L for specimens thinner than 20 μm.

In addition to the circuit parameters, the high-frequency impedance characteristic of the specimen is strongly affected by the cavity resonance. The resonant frequency $f_{\rm cav}$ depends on the resonator length l and the square root of the dielectric constant. To determine l, we analyzed the electric field associated with the fundamental mode propagating in the specimen. The magnitude of the electric field has radial symmetry with a maximum in the center of the specimen. In general, the magnitude of the electric field decreases along the radius, reaching a minimum at a distance smaller than the radius of the specimen. The fundamental mode propagates along the diameter of the specimen rather than along its thickness. The value of l was obtained from the propagation term of (1) by putting $\omega l\sqrt{\varepsilon^*}/2c = \pi$ and using $f_{\rm cav}$ values calculated by HFSS. For the APC-7 configuration, we estimated that the value of l is about 2.4 mm and apparently does not depend on the specimen dielectric permittivity. Calculations for other coaxial configurations indicate that the resonator length is smaller than the physical diameter of the specimen by a factor of about 0.8.

Having determined the residual inductance and the resonator length, one can calculate input impedance $Z_{\rm in}$ from (1). Equation (1) agrees well with HFSS results and correctly predicts the impedance characteristic at frequencies of up to the first cavity resonance. In the case of specimens with a permittivity of 69.2, the frequency of the first cavity resonance is about 14.6 GHz. For higher order resonances there is only qualitative agreement between (1) and the results simulated by HFSS.

B. Experimental Results

In order to verify our numerical results we measured the scattering parameter S_{11} of water as a high dielectric constant material. The simulation was performed using dielectric parameters from Ansoft library with the dielectric constant $\varepsilon\prime$ of 76 at 30 °C, conductivity of 2 μS/cm, and no dispersion. The inductance L determined from (2) is about 30 pH.

Fig. 5 compares the input impedance of a 240 μm thick water film measured at 30 °C with that calculated from (1). It is seen that the calculated impedance magnitude and phase are in good agreement with the experimental results. The impedance characteristic exhibits a minimum at the resonant frequency $f_{\rm LC}$ of about 4.67 GHz accompanied by the corresponding phase change. As the frequency increases above 9 GHz there is noticeable discrepancy between the calculated and measured results mainly due to growing dielectric dispersion of water, which exhibits a single relaxation process with a maximum at the relaxation frequency of about 22 GHz [14]. This causes the dielectric constant to decrease with frequency and considerably shifts the $f_{\rm cav}$ to higher frequencies. Overall the presented example and results obtained for other dielectrics, including air, demonstrate good correlation between calculated and experimental data at frequencies of up to 10 GHz, which is almost one order of magnitude higher than the 1.5 GHz frequency limit for the lumped capacitance method. Considering the constraints in calibrating the experimental test fixture above 10 GHz and the uncertainty in measuring the thickness of the gap, the results of determining impedance are well within the tolerances in measuring the scattering parameter. It is noteworthy that (1) can be applied to materials with dielectric dispersion and solved by using an iterative algorithm.

IV. Conclusion

We have obtained a complete numerical solution for input impedance of a film specimen terminating a coaxial line. In contrast to the existing lumped capacitance approximations, we formulated the problem without prior assumptions about the network equivalent circuit. Using results from the numerical simulations, we formulated a practical expression for the input impedance of complex gap capacitance terminating a coaxial transmission line. The impedance characteristic of such a network is affected by the *LC* resonance coupled with the cavity resonance. The residual inductance of the specimen is linearly dependent on the specimen thickness. At frequencies near the cavity resonance, the specimen section represents a network consisting of a transmission line with a capacitance, where the fundamental mode propagates along the diameter of the specimen. In contrast to the existing solutions, which are applicable to frequencies below the first series resonance, our model expression (1) is accurate in a wider frequency range, up to the first cavity resonance. Using water as a high dielectric constant material, we have demonstrated that there is good agreement between the model expression and experimental data in the APC-7 configuration, up to a frequency of about 10 GHz.

We consider our analysis a significant step toward improved understanding of wave propagation in coaxial discontinuities, particularly since the distribution of the electromagnetic field inside such structures is usually difficult to examine experimentally. Results of our analysis can be utilized to conduct more accurate broadband dielectric measurements of thin films with high dielectric constant at higher, microwave frequencies, which are of interest to bio-and nanotechnology.

References

[1] A. M. Tsai, D. A. Neuman, and L. H. Bell, "Molecular dynamics of solid-state Lysozyme as affected by glycerol and water: A neutron scattering study," *Biophys. J.*, vol. 79, pp. 2728–2732, 2000.

[2] M. F. Iskander and S. S. Stuchly, "Fringing field effect in the lumped-capacitance method for permittivity measurements," *IEEE Trans. Instrum. Meas.*, vol. IM-27, pp. 107–109, 1978.

[3] M. A. Stuchly and S. S. Stuchly, "Coaxial line reflection methods for measuring dielectric properties of biological substances at radio and microwave frequencies: A review," *IEEE Trans. Instrum. Meas.*, vol. IM-29, pp. 176–183, 1980.

[4] *Waveguide Handbook*, McGraw-Hill, New York, NY, 1951. N. Marcuvitz.

[5] J. Obrzut, N. Noda, and R. Nozaki, "Broadband characterization of high-dielectric constant films for power-ground decoupling," *IEEE Trans. Instrum. Meas.*, vol. 51, pp. 829–832, 2002.

[6] H. J. Eom, Y. C. Noh, and J. K. Park, "Scattering analysis of a coaxial line terminated by a gap," *IEEE Microwave Guided Wave Lett.*, vol. 8, pp. 218–219, 1998.

[7] M. V. Davidovich, "Full-wave analysis of coaxial mounting structure," *IEEE Trans. Microwave Theory Tech.*, vol. 47, pp. 265–270, Mar. 1999.

[8] J.-F. Lee, D.-K. Sun, and Z. J. Cendes, "Full-wave analysis of dielectric waveguides using tangential vector finite elements," *IEEE Trans. Microwave Theory Tech.*, vol. 39, pp. 1262–1271, Aug. 1991.

[9] J. Obrzut and A. Anopchenko, "High-frequency input impedance characterization of dielectric films for power-ground planes," *IEEE Trans. Instrum. Meas.*, vol. 52, pp. 1120–1124, Aug. 2003.

[10] N.-E. Belhadj-Tahar, O. Dubrunfaut, and A. Fourrier-Lamer, "Equivalent circuit for coaxial discontinuities filled with dielectric materials—Frequency extension of the Marcuvitz's circuit," *J. Electromagn. Wave*, vol. 15, pp. 727–743, 2001.

[11] A. Lian and W. Zhong, "An improved lumped capacitance method for dielectric measurements," *J. Mater. Sci.*, vol. 25, pp. 4349–4355, 1990.

[12] M. S. Navarro, "Disk-gap discontinuity in a coaxial transmission line," *Circuits Syst.*, vol. 2, pp. 735–738, 1991.

[13] J. Chramiec and J. K. Piotrowski, "Universal formula for frequency-dependent coaxial open-end effect," *Electron. Lett.*, vol. 35, pp. 1474–1475, 1999.

[14] J. B. Hasted, *Aqueous Dielectrics*. London, U.K.: Chapman and Hall, 1973, p. 43. Tab. 2.1.

J. Obrzut received the Ph.D. degree in technical sciences from the Institute of Physics, Cracov Polytechnic, Poland, in 1981.

After a postdoctoral appointment at the Polymer Science Department, University of Massachusetts, he was a Researcher at the Five College Radio Astronomy Department, Amherst, MA, working on microwave dielectric waveguides. He joined IBM in 1988 as Advisory Engineer where he was conducting exploratory work on application of polymer dielectrics in microelectronics. He has been with the NIST Polymers Division since 1997, where he pursues research in metrology of dielectric films and hybrid materials for microwave and electronic applications. His research interests include embedded passive devices and organic electronic materials.

A. Anopchenko was born in Nizhnevartovsk, Russia, in 1970. He graduated from Kharkov Polytechnic Institute, Ukraine, in 1993 and received the Ph.D. degree in solid-state physics from Comenius University, Bratislava, Slovakia, in 2001.

He was an Engineer at B. I. Verkin Institute for Low Temperature Physics and Engineering, National Academy of Sciences, in 1993–1997 and was a Research Associate at the Institute of Physics, Slovak Academy of Sciences, in 1997–2001. Since 2001, he has been a Guest Researcher at the Polymers Division, National Institute of Standards and Technology, Gaithersburg, MD. His current research interests includes analysis of discontinuities in transmission lines, simulations of high-frequency electromagnetic field distribution in three-dimensional structures, application of microwave techniques for broadband permittivity measurements of polymer composites and biological substances, dielectric properties and molecular dynamics of glass formers, x-ray scattering techniques, and low-dimensional and interfacial phenomena.